ZNF667 facilitates angiogenesis after myocardial ischemia through transcriptional regulation of VASH1 and Wnt signaling pathway

WENMEI WANG[1-3], WEITE SHANG[1,2], JIANG ZOU[1,2], KE LIU[1,2], MEIDONG LIU[1,2], XIAOQIN QIU[3], HUALI ZHANG[1,2], KANGKAI WANG[1,2] and NIAN WANG[1,2,4]

[1]Department of Pathophysiology, School of Basic Medical Science, [2]Key Laboratory of Sepsis Translational Medicine of Hunan, Central South University; [3]Department of Pathology, Xiangya Hospital, Central South University; [4]Research Center of China-Africa Infectious Diseases, Xiangya School of Medicine, Central South University, Changsha, Hunan 410008, P.R. China

Received March 16, 2022; Accepted August 9, 2022

DOI: 10.3892/ijmm.2022.5185

Abstract. Zinc finger protein 667 (ZNF667, also referred as Mipu1), a widely expressed KRAB/C_2H_2-type zinc finger transcription factor, can protect against hypoxic-ischemic myocardial injury. Pro-angiogenesis is regarded as a promising strategy for the treatment of acute myocardial infarction (AMI). However, whether ZNF667 is involved in the angiogenesis following AMI remains to be elucidated. The present study reported that the expression of ZNF667 in CD31-positive endothelial cells (ECs) was upregulated in the heart of AMI mice. Hypoxic challenge (1% oxygen) promoted the mRNA and protein expression of ZNF667 in the human umbilical vein endothelial cells (HUVECs) in a time-dependent manner. Moreover, ZNF667 promoted hypoxia-induced invasion and tube formation of HUVECs. Mechanically, ZNF667 could directly bind to the promoter of anti-angiogenic gene VASH1 and inhibit its expression. Consequently, VASH1 overexpression abolished hypoxic challenge or ZNF667 overexpression-induced invasion and tube formation of HUVECs. Further bioinformatic analyses suggested that overexpression of ZNF667 or knockdown of VASH1-induced differentially expressed genes in HUVECs were greatly enriched in the Wnt signaling pathway (*DAAM1*, *LEF1*, *RAC2*, *FRAT1*, *NFATc2* and *WNT5A*). Together, these data suggested that ZNF667 facilitates myocardial ischemia-driven angiogenesis through transcriptional repression of VASH1 and regulation of Wnt signaling pathway.

Correspondence to: Dr Nian Wang or Dr Kangkai Wang, Department of Pathophysiology, School of Basic Medical Science, Central South University, 111 Xiangya Road, Changsha, Hunan 410008, P.R. China
E-mail: wangnian@csu.edu.cn
E-mail: wangkangkai@csu.edu.cn

Abbreviations: siRNA, small interfering RNA; AMI, acute myocardial infarction; LAD, left anterior descending coronary artery; MVD, microvessel density; HUVEC, human umbilical vein endothelial cells; IHD, ischemic heart disease; ZNF667, zinc finger protein 667; EC, endothelial cell; ChIP, chromatin immunoprecipitation; EMSA, electrophoretic mobility shift assay; VASH1, vasohibin 1; Mipu1, myocardial ischemic preconditioning upregulated protein 1

Key words: zinc finger protein 667, vasohibin 1, Wnt signaling pathway, angiogenesis, acute myocardial infarction

Introduction

Ischemic heart disease (IHD), also referred to as the coronary artery disease, is one of the most common diseases and has been the leading cause of mortality and disability worldwide in the last two decades (1,2). The major causes of IHD are atherosclerosis, atherosclerotic plaque rupture and thrombosis in the coronary arteries, which lead to low perfusion in the region supplied by the occluded vessels. Decreased blood flow can induce myocardial hypoxic injury. Due to the intrinsic inability of myocardium to regenerate, it fails to self-rehabilitate following myocardial infarction. Persistent ischemia can ultimately result in irreversible myocardial injury, remodeling of the remaining non-infarcted myocardium and even heart failure (3,4). Early restoration of blood supply to the ischemic myocardium may improve the prognosis of patients with IHD.

Cardiac angiogenesis is an essential regenerative event in the ischemic injured hearts following acute myocardial infarction (AMI) and *de novo* formation of microvessels salvages the ischemic myocardium at the early stage (5). However, compelling evidence suggests that cardiac angiogenesis following ischemia is inadequate, which may promote irreversible transition from adaptive cardiac hypertrophy to cardiac dysfunction. Consequently, pro-angiogenic therapy, which generates new blood vessels from existing vasculature, appears to be a promising strategy for the treatment of IHD. To date, various pro-angiogenic strategies have emerged, including targeted delivery of pro-angiogenic factors, implantation of stem cells and targeted genome engineering (6-10). Although the pro-angiogenic effects of these methods are appealing, there are limitations and concerns, such as delivery modality, uncontrolled angiogenesis, limited half-life of growth factors and effects on other organs (6-10).

Hence, exploring novel endogenous pro-angiogenic mediators is of great importance.

Angiogenesis is a co-regulated and balanced process of pro-angiogenic factors [e.g., vascular endothelial growth factor A (VEGFA), fibroblast growth factor 2 (FGF2) and hepatocyte growth factor (HGF)] and anti-angiogenic factors [e.g., angiostatin, vasohibin 1 (VASH1) and thrombospondins (TSP)] (7,11-13). To date, numerous studies have been conducted to understand the roles of these angiogenic factors in the pro-angiogenic and anti-angiogenic therapy (11,12,14-16). However, the regulation of these gene expressions during angiogenesis has not been extensively elucidated. Increasing attention focuses on various transcription factors (TFs) that are expressed in the endothelial cells (ECs) during vascular development. TFs bind to specific DNA sequences within the promoter regions, form a complex with different co-regulatory proteins and thus result in transcriptional activation or repression of genes. It has been reported that multiple TFs, such as hypoxia-inducible factor (HIF)-1, Sp1 transcription factor (SP1), transcription factor AP-2 α (TFAP2A), early growth response 1 gene (EGR1), signal transducer and activator of transcription 6 (STAT6) and estrogen-related receptor γ (ERRγ) can transcriptionally regulate VEGF family members by directly interacting with specific binding sites on their promoter sequences (17-19). In addition, ischemia-hypoxia can drive the transcription of various anti-angiogenic factors by different TFs, such as EGR1, JUN and enhancer of zeste 2 polycomb repressive complex 2 subunit (EZH2) (20).

Zinc finger protein 667 (ZNF667) was previously named as myocardial ischemic preconditioning upregulated protein 1 (Mipu1). It was first identified by our laboratory in 2004 as it is upregulated during myocardial ischemic preconditioning (21). ZNF667 is a Krüppel-associated box (KRAB)/C_2H_2-type zinc finger transcription factor and exerts remarkable cardioprotective functions. For instance, ZNF667 can protect against H_2O_2-induced apoptosis of cardiomyocytes through transcriptional inhibition of Bax and Fas (22,23). Moreover, ZNF667 has a transcriptional repressive effect on SRE and JUN in the mitogen-activated protein kinase signaling pathway in the H9c2 cardiomyoblasts (24). It is worth noting that ZNF667 contributes to HIF1A-mediated cytoprotective effects through inhibiting the transcription of pro-apoptotic gene BAX and activating mitochondrial apoptotic pathway (25). It is known that HIF1A can potentially activate the transcription of various angiogenesis-related factors in response to hypoxia and participate in every step of angiogenesis (26). However, whether ZNF667 is involved in the angiogenesis following myocardial ischemia through transcriptional regulation of angiogenesis-related factors is largely unknown. Hence, the present study investigated the effect of ZNF667 on angiogenesis following AMI and its potential mechanisms.

Materials and methods

Establishment of mouse model of AMI. A total of 34 male 8-week-old C57BL/6J mice (20-25 g) were purchased from the Center of Experimental Animals in Central South University of China and randomly divided into two groups: sham-operated group and LAD group (n=17 per group). The mice were kept in a controlled environment with 12-h light/dark cycle, room temperature of 20±2˚C, and humidity of 55±10%. They were housed individually with free access to food and water throughout the experiment. Animal use procedures were approved by the animal welfare ethics committee of Central South University (approval no. 20131502). In addition, all animal protocols conform to the Guide for the Care and Use of Laboratory Animals (8th edition) published by the US National Institute of Health (27). An experimental mouse model of MI was established by permanently ligating the left anterior descending (LAD) coronary artery according to previously reported protocols (28). In brief, anesthesia was induced with 4% isoflurane (800 ml O_2/min) and maintained by endotracheal ventilation of 2-3% isoflurane (800 ml O_2/min). Under sterile conditions, the mouse heart was exposed through left thoracotomy at the fourth intercostal space and the LAD was ligated with a 7-0 suture. The thoracic incision was closed following ST-segment elevation observed in an electrocardiogram. Mice were extubated when breathing was restored. To test the effects of surgery alone, the suture was passed around the coronary artery but not ligated in the sham group. Then, the performance of left ventricle (LV) was measured in mice under inhalational anesthesia with 2-3% isoflurane (800 ml O_2/min). A small cannula filled with heparin saline (500 U/ml) was inserted into the LV through the apex with chest open and mechanically ventilated and positioned along the cardiac longitudinal axis. After stabilization for 2 min, the pressure signal was continuously recorded using a MacLab A/D converter (ADInstruments). The left ventricular systolic pressure (LVSP) and left ventricular end-diastolic pressure (LVEDP) were measured and the maximal slope of systolic pressure increment (+dp/dt) and diastolic pressure decrement (-dp/dt) were calculated. Mice were anaesthetized through isoflurane (2%) inhalation (800 ml O_2/min) and then sacrificed by cervical dislocation on day 1, 3, 7 and 14 following LAD operation.

Measurement of myocardial infarct size. The myocardial infarct size was measured by 2% triphenyltetrazolium chloride (TTC) staining as described previously (28). Positive TTC staining was in red color, and the infarcted area was pale. Images were analyzed by Image-Pro Plus 6.0 (Media Cybernetics, Inc.), and the infarct size was expressed as a percentage of ischemic area at risk (% IAR).

Histology and immunohistochemistry (IHC) staining. Mice were sacrificed on day 1, 3, 7 and 14 after surgery, the hearts were harvested and fixed in 4% paraformaldehyde overnight at 4˚C and then embedded in paraffin for sectioning according to standard protocols. Tissue sections at 5 μm thickness were mounted on a Superfrost Plus glass slide at 42-55˚C, dried at 60˚C for 2 h and used for hematoxylin and eosin (H&E; room temperature for 5 and 2 min, respectively) and IHC staining (primary antibody at 4˚C overnight and second antibody at room temperature for 1, respectively). Antibodies were used as follows: anti-CD31 antibody (Wuhan Servicebio Technology Co., Ltd.; cat. no. GB11063-2; 1:300 dilution), anti-ZNF667 antibody (Abcam; cat. no. ab106432; 1:800 dilution) and anti-VASH1 antibody (Bioworld Technology, Inc. technology; cat. no. BS8509; 1:400 dilution). Microvessel density (MVD) was calculated by identifying 3 fields from area of highest

vascular density in the ischemic myocardium per slide of each sample and counting at low power lens (magnification, x200) (29). Images were captured using automatic digital slide scanning system (KFBIO). A total of five random fields per section were analyzed using Image Pro-Plus 7.0 software (Media Cybernetics, Inc.) in a double-blind fashion to analyze the percentage of positive expression.

Cell culture. Human umbilical vein endothelial cell line (HUVECs) was purchased from the American type culture collection (cat. no. CRL-1730) and cultured in Dulbecco's Modified Eagle Medium (DMEM; HyClone; Cytiva) supplemented with 10% fetal bovine serum (FBS), 100 μg/ml streptomycin, 100 U/ml penicillin, 0.03 mg/ml endothelial cell growth supplements and 0.1 mg/ml heparin (MilliporeSigma). Cells were maintained at 37˚C in a humidified atmosphere containing 95% air and 5% CO_2. For hypoxic conditions, cells were cultured at 37˚C in a humidified temperature-controlled incubator (Don Whitley Scientific Ltd.) containing 5% CO_2, 94% N_2 and 1% O_2. Cells were trypsinized and resuspended in DMEM after they reached confluency.

Transient transfection. Plasmid pcDNA3.1-ZNF667, pcDNA3.1-VASH1 and control vector pcDNA3.1 were constructed by our lab as previously described (24,30). The plasmid was diluted in Opti-MEM (Gibco; Thermo Fisher Scientific, Inc.) and mixed with MegaTran 1.0 transfection reagent (OriGene Technologies, Inc.) according to the manufacturer's instructions. In brief, HUVECs were seeded in a 6-well plate at a density of $5x10^4$ cells/well 24 h prior to transfection. When the cells reached 70% confluence, 1.5 μg of plasmid was diluted in 100 μl of Opti-MEM and then 4.5 μl of MegaTran 1.0 was added to the diluted plasmid. The MegaTran 1.0/plasmid mixture was vortexed for 10 seconds, incubated at room temperature for 10 min and gently added to different wells that already contained about 900 μl of DMEM medium. The siRNA sequences used for this study were as follows: scramble siRNA (sense: 5'-GAGUUGAAAUCUACUGGUCAUUA-3'; anti-sense: 5'-UAAUGACCAGUAGAUUUCAACUC-3'), ZNF667 siRNA (sense: 5'-CUUCAUCAGAACAUUCAUA-3'; anti-sense: 5'-UAUGAAUGUUCUGAUGAAG-3') and VASH1 siRNA (sense: 5'-GCUGUGCAGCGCUACAUCA-3'; anti-sense: 5'-UGAUGUAGCGCUGCACAGC-3'). SiRNAs were diluted in Opti-MEM and mixed with Lipofectamine® 3000 (Invitrogen; Thermo Fisher Scientific, Inc.) according to the manufacturer's instructions. At 48 h after transfection, cells were incubated either in normoxic or hypoxic condition.

Reverse transcription-quantitative (RT-q) PCR. Total RNA from $5x10^5$ cells was extracted using the TRIzol® reagent (Thermo Fisher Scientific, Inc.) and reverse transcribed to cDNA using PrimeScript RT reagent kit (Takara Bio, Inc.). The mRNA expression was detected by SYBR® Premix Ex Taq (Takara Shuzo Co.) using ABI 7500 real-time PCR system (Thermo Fisher Scientific, Inc.). PCR cycling conditions were as follows: Initial denaturation at 94˚C for 5 min; followed by 35 cycles of denaturation at 94˚C for 30 sec, annealing at 55˚C for 30 sec and extension at 72˚C for 30 sec. Relative quantitation of mRNA was analyzed using the equation as follows: Ratio=$2^{-\Delta\Delta Cq}$ and normalized using *ACTB* gene (31). All the experiments were repeated three times. Primers used in this study are listed in Table I. All procedures including RNA extraction, cDNA synthesis, and qPCR were performed according to the manufacturer's instructions.

RNA sequencing (RNA-seq). Total RNA from HUVECs transfected with pcDNA3.1 or pcDNA3.1-ZNF667 plasmid was extracted using TRIzol® reagent (Thermo Fisher Scientific, Inc.) and the quality and integrity [RNA Integrity Number (RIN)>8.1] of RNA was verified by a Bioanalyzer. Each sample had three biological replicates that were processed in separate batches. RNA-seq library preparation and Illumina sequencing were performed using HiSeq 2500 platform (Beijing Genomics Institute). An average of 20±0.5 million reads were produced from each sample for minimal sequencing coverage. The raw data files containing reads and quality scores have been uploaded to the Gene Expression Omnibus (GEO) database: GSE208105 (https://www.ncbi.nlm.nih.gov/geo/query/acc.cgi?acc=GSE208105).

Immunoblotting. Myocardial tissues and HUVECs were homogenized or scraped using radioimmunoprecipitation assay (RIPA) buffer [150 mM NaCl, 1% Triton X-100, 1% sodium deoxycholate, 0.1% SDS, 50 mM Tris-HCl (pH 7.5) and 2 mM EDTA (pH 8.0)] supplemented with protease inhibitors. The lysate was centrifuged at 14,000 x g for 10 min at 4˚C and then the protein concentration was quantified by the Bradford method. Protein samples were then mixed with 5X loading buffer. Equal amounts of protein (20-50 μg) were loaded on 10% sodium dodecyl-sulfate polyacrylamide gel electrophoresis (SDS-PAGE) and then transferred to polyvinylidene fluoride membranes (Millipore). After blocking with 5% non-fat milk (diluted in Tris-buffered saline with Tween 20) for 2 h, membranes were incubated with different primary antibodies at 4˚C overnight. The following antibodies were used for immunoblotting: Anti-GFP antibody (Cell Signaling Technology, Inc.; cat. no. 2555S; 1:1,000 dilution), anti-VASH1 antibody (Bioworld Technology, Inc.; cat. no. BS8509; 1:1,000 dilution), anti-GADPH antibody (Millipore; cat. no. G9545; 1:3,000 dilution). Subsequently, the membranes were incubated with HRP-labeled Goat Anti-Rabbit IgG (H + L) (Beyotime Institute of Biotechnology; cat. no. A0208; 1:5,000 dilution) or HRP-labeled Goat Anti-Mouse IgG (H + L) (Beyotime Institute of Biotechnology; cat. no. A0216; 1:5,000 dilution) at room temperature for 1 h. Enhanced chemiluminescence (ECL) was performed by using Clarity Max Western ECL Substrate (Bio-Rad Laboratories, Inc.; cat. no. 1705062). The relative band intensity was calculated using Image Pro-Plus 7.0 software (Media Cybernetics, Inc.). GAPDH was used as a loading control for protein normalization.

Chromatin immunoprecipitation-quantitative PCR. Chromatin immunoprecipitation (ChIP) assay was performed using the ChIP assay kit (Beyotime Institute of Biotechnology; cat. no. P2078) according to the manufacture's protocol. Before ChIP assay, the potential binding sites in the promoters of 10 angiogenesis-related genes were predicted using the JASPAR database (http://jaspar.genereg.net/), in which the scores of predicted binding sites ≥8.0 and relative scores of predicted binding sites ≥0.8 were screened out and further identified

Table I. Primer sequences of target genes for reverse transcription-quantitative PCR

Gene	Accession number	Forward primer (5' to 3')	Reverse primer (5' to 3')
VASH1	NM_014909	CAAATGCCTGGAAGCCGTGATC	AGCACGATGTGGCGGAAGTAGT
DAAM1	NM_001270520	ATTCCTCAGCCCACAAATGCCC	GCAGAGAAGGTTCTTTCCAGGTC
LEF1	NM_016269	CTACCCATCCTCACTGTCAGTC	GGATGTTCCTGTTTGACCTGAGG
RAC2	NM_002872	CAGCCAATGTGATGGTGGACAG	GGAGAAGCAGATGAGGAAGACG
FRAT1	NM_005479	TCCCAACCAGAAACCCGCACAG	TAACTGCAGCCGTCGCGAATGA
PLCB2	XM_017022317	CCTGGAAGTGACGGCTTATGAG	GCTCTGTGAAGGACGAGATGAC
AXIN2	NM_004655	CAAACTTTCGCCAACCGTGGTTG	GGTGCAAAGACATAGCCAGAACC
NFATC2	NM_001258297	GATAGTGGGCAACACCAAAGTCC	TCTCGCCTTTCCGCAGCTCAAT
CXXC4	NM_025212	TGCCCGCAGAATCATTCCTCCT	ACGCCACAGTTGATGAGCCTCT
WNT5A	NM_003392	TACGAGAGTGCTCGCATCCTCA	TGTCTTCAGGCTACATGAGCCG
ZNF667	NM_001321356	AAACCCCGTCTCCACTGAAAAA	CAAGCGATTCTTCTCCTTCAGC
ACTB	NM_001101	CACCATTGGCAATGAGCGGTTC	AGGTCTTTGCGGATGTCCACGT

by ChIP assay and qPCR. A total number of $5x10^6$ HUVECs were crosslinked, resuspended and lysed in 10 ml cell culture medium containing 37% formaldehyde, then sonicated to shear the DNA into a range of 400-800 bp. The chromatin fraction was then immunoprecipitated using ZNF667 antibody (Abcam; cat. no. ab106432, 1:50 dilution) or IgG antibody (Abcam; cat. no. ab172730, 1:50 dilution) at 4˚C overnight. Then the mixture was incubated with protein A + G agarose beads at 4˚C for 1 h, which was isolated and washed sequentially by sequentially, high salt immune complex wash buffer, LiCl immune complex wash buffer, TE buffer. Purified DNA was then subjected to qPCR as described above using primers near the specific DNA binding site 5'-TGTCTTATCGAA-3' in the ZNF667 promoter. The detection of a band on agarose gel electrophoresis indicated the presence of binding between the transcription factor and target genes. The percentage of input was calculated and normalized by IgG as a fold change. Primers for ChIP analysis were as follows: VEGFA-forward: 5'-TAGCAAAGAGGGAACGGCTC-3'; reverse: 5'-AACTCT GTCCAGAGACACGC-3'; PFKFB3-forward: 5'-CTTGTC GCTGATCAAGGTGA-3'; reverse: 5'-TAGTACACGATG CGGCTCTG-3'; VASH1-forward: 5'-AGGACCGGAAGA AGGATGTT; reverse: 5'-TGGTACCCGTTAAGGTCTGG-3'.

Electrophoretic mobility shift assay (EMSA). The DNA-protein interaction was analyzed using LightShift Chemiluminescent EMSA kit (Thermo Fisher Scientific, Inc.; cat. no. 20148) according to the manufacturer's instructions. DNA probes were generated according to sequences between -226 to -222 bp upstream of the transcription start site (TSS) of human VASH1 promoter as double-stranded, biotin-labeled oligonucleotides corresponding to the wild type sequences (5'-AGGGGGAGCATCTTAAAGCAC ACAC-3') and mutant sequence (5'-AGTGGGAGCATA GTAAAGCACACAC-3'). Specific binding was confirmed using 100-fold excess of unlabeled mutant oligonucleotides (mutant cold probe) and 100-fold excess of unlabeled identical oligonucleotides (cold probe), respectively. The nuclear extract was incubated with different oligonucleotides at room temperature for 20 min before being separated on a 6% non-denaturing acrylamide gel. Target bands were detected by ECL mentioned above.

Matrigel-based tube formation assay. Tube formation assay was performed as reported previously (29). Firstly, Matrigel matrix (BD Biosciences; cat. no. 354234) was fully dissolved at 4˚C overnight. Then, 50 μl of Matrigel matrix was added to 96-well plates and incubated at 37˚C for 30 min. Next, $3\text{-}5x10^3$ HUVECs in 150 μl of cell culture medium were seeded on the Matrigel in each well. The tubular formation of HUVECs in five random fields were imaged using an inverted-phase contrast microscope. The number of tubules, loops and branch points were quantified using online tool WimTube (Wimasis, Onimagin Technologies SCA).

Scratch wound healing assay. A total of $2x10^5$ HUVECs were plated in each well of 6-well plates. After the cells were adherent to the plate, a 10 μl sterile pipette tip was used to scratch at the middle of each well. Invasion was determined by visual assessment of cells that had repopulated wound margins using phase-contrast microscopy. The distance of the scratch was measured using ImageJ (National Institutes of Health) at 0 and 24 h following incubation and relative invasion distance was compared with the control group (e.g., scramble siRNA or pcDNA3.1 group). The total amount of invasion was calculated by subtracting the final invasion area for each image.

Bioinformatics analysis of RNA-seq data and GEO arrays. Microarray data set: RNA-seq for ZNF667 overexpression was completed in the Beijing Genomics Institute as mentioned above (GSE208105). RNA-seq data of VASH1 knockdown was obtained from publicly available Gene Expression Omnibus (GEO) database GSE27871. Wilcoxon rank-sum test was used to determine the differentially expression genes (DEGs) between the above groups. Transcripts were further filtered by fold change ≥ 2, $P<0.05$. Biological insights from candidate genes were obtained by performing Gene Ontology (GO) (biological processes) enrichment and Kyoto Encyclopedia of Genes and Genomes (KEGG) analysis.

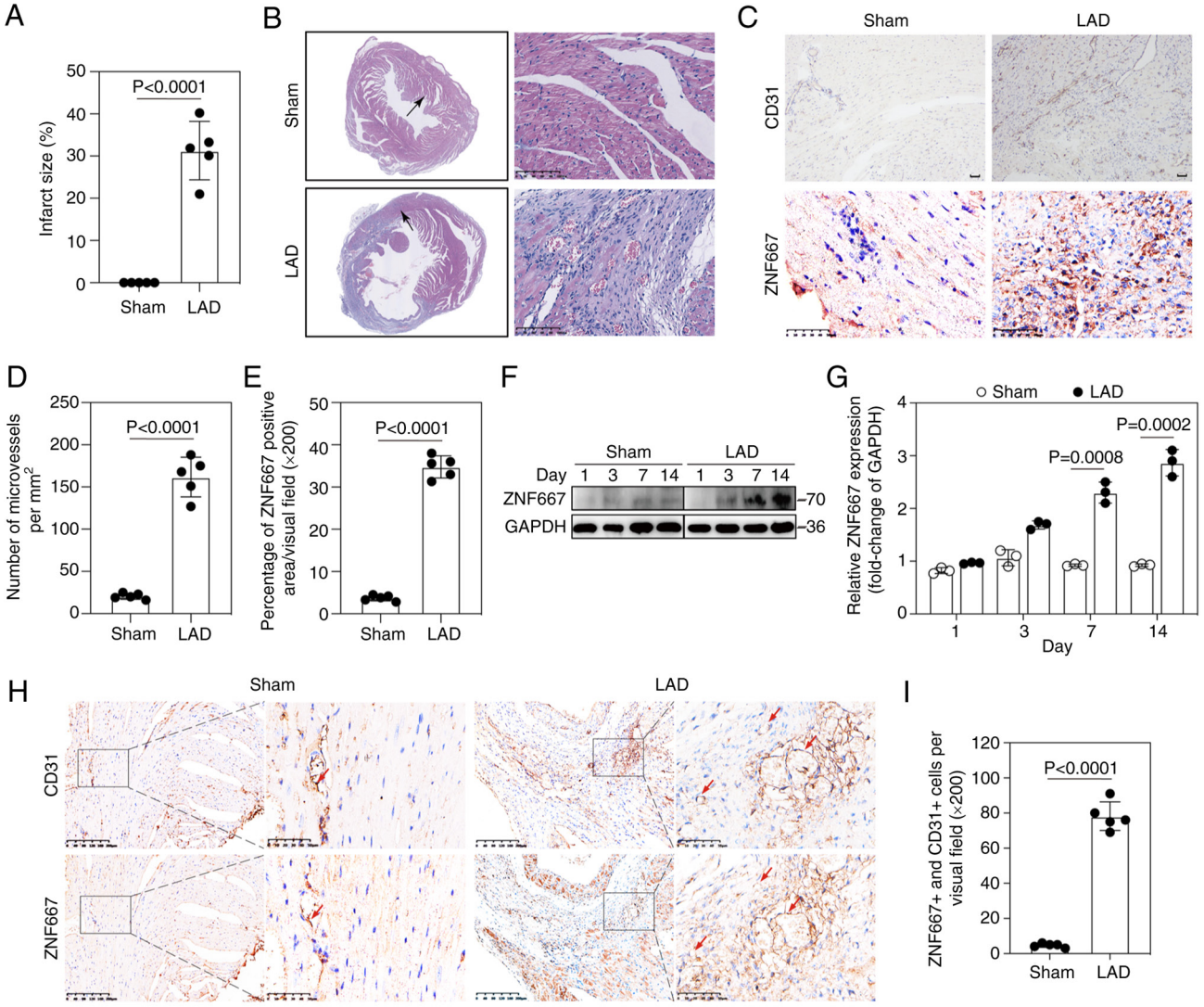

Figure 1. The expression of ZNF667 and angiogenesis were increased in the ischemic myocardium of AMI mice. (A) The statistics histogram of myocardial infarct size of mice on day 14 after LAD ligation (n=5 per group). (B) Morphological and pathological changes of myocardium were observed by hematoxylin and eosin staining on day 14 following surgery (Scale bar=100 μm). (C) The expression of CD31 (upper) and ZNF667 (lower) in the ischemic myocardium (left ventricle) of mice was detected by immunohistochemistry on day 14 following surgery (Scale bar=50 μm). (D) Microvessel density was calculated by identifying five fields from an area of highest vascular density in the ischemic myocardium per slide of each sample and counting at low power lens (n=5 per group). (E) The statistics histogram of positive expression of ZNF667 in the ischemic myocardium (left ventricle) of mice (n=5 per group). (F) Expression of ZNF667 in the left ventricle of mice on day 1, 3, 7 and 14 following surgery was detected by immunoblotting. (G) Quantification of immunoblot analysis of ZNF667 (n=3 per group). (H) The expression of CD31 and ZNF667 in the serial ischemic myocardium sections of AMI mice on day 14 following surgery were detected by immunohistochemistry. Scale bar (left)=200 μm, (right)=50 μm. The arrows indicate the co-localization of positive expression of CD31 and ZNF667. (I) Quantification of positive expression rate of ZNF667 in CD31-positive cells in the ischemic myocardium of AMI mice (n=5 per group). Data are presented as mean ± standard deviation. ZNF667, zinc finger protein 667; AMI, acute myocardial infarction; LAD, left anterior descending coronary artery.

Statistical analysis. All statistical analyses were performed using GraphPad Prism 7.0 (GraphPad Software, Inc.) software. Measurement data were represented as mean ± standard deviation. Differences among groups were determined by one-way analysis of variance (ANOVA). Post hoc test was performed using the least significant difference (LSD) test when ANOVA was significant. Differences between two groups were analyzed by unpaired Student's t-tests. P<0.05 was considered to indicate a statistically significant difference.

Results

ZNF667 is highly expressed in the ECs of ischemic myocardium following AMI. To investigate the role of ZNF667 in angiogenesis following myocardial ischemia, a mouse model of AMI was established through LAD ligation (Figs. 1A and S1A). On day 14 after LAD ligation, the AMI mice developed severe left ventricular wall thinning, extensive fibrosis and abnormal cardiac hemodynamics when compared with the sham-operated controls (Figs. 1B and S1B-G). To assess the neovascularization of ischemic myocardium, the expression of endothelial markers, such as CD31, was detected in the ischemic myocardium and then microvessel density (MVD) based on CD31-positive ECs was calculated. The results showed that MVD was prominently increased in the ischemic myocardium (Fig. 1C-E). In addition, the expression of ZNF667 in the ischemic myocardium increased with the extension of ischemic time and reached a peak on day 14 after

LAD ligation (Fig. 1F and G). The expression of ZNF667 in the ECs was further detected by IHC using serial sections. As shown in Fig. 1H and I, ZNF667 showed marked co-localization with CD31 and the expression of ZNF667 in CD31-positive ECs was higher than that in the sham controls (Fig. 1G). These data indicated that ZNF667 was highly expressed in the ECs within the ischemic myocardium and might be involved in neovascularization following an AMI.

ZNF667 mediates hypoxia-induced invasion and tube formation of HUVECs. HUVECs exposed to hypoxic condition (1% O_2) were used to mimic the ischemic situation *in vivo*. It was found that hypoxia increased both, the mRNA and protein expression, of ZNF667 in a time-dependent manner (Fig. 2A-C). As shown in Fig. 2F and G, hypoxia exposure significantly promoted the invasion and tube formation of HUVECs. However, downregulation of ZNF667 expression by siRNA mitigated hypoxia-enhanced invasion and tube formation of HUVECs (Fig. 2D, H, I, L and M). Moreover, overexpression of ZNF667 evidently enhanced invasion and tube formation of HUVECs exposed to normoxic conditions (Fig. 2E, J, K, N and O). These data further indicated that ZNF667 could mediate ischemia- or hypoxia-induced angiogenesis.

ZNF667 inhibits the transcription of VASH1 through directly binding to its promoter. As a KRAB/C_2H_2-type zinc finger transcription factor, ZNF667 exerts its function mainly through binding to specific core sequence 5'-CTTA-3' in the promoter regions of different target genes (23). Bioinformatic prediction was hence used to screen out angiogenesis-related target genes of ZNF667. The present study predicted and evaluated the potential binding sites in the promoters of 10 angiogenesis-related genes (VEGFA, VASH1, SVBP, PFKFB3, FGF2, KDR, FLT1, ANGPT1, ANGPT12 and TEK) using the JASPAR database (http://jaspar.genereg.net/), in which the scores of predicted binding sites ≥8.0 and relative scores of predicted binding sites ≥0.8 were screened out and further identified by ChIP assay and qPCR (Table SI). Finally, three angiogenesis-related genes that have ZNF667 binding sites in their promoters were screened out as candidate target genes of ZNF667, including VEGFA, VASH1 and PFKFB3. Multiple putative ZNF667 binding sites were found in the promoter region of VEGFA (-491 to -485; -614 to -608; -1123 to -1117), VASH1 (-154 to -148; -226 to -220) and PFKFB3 (-214 to -208; -689 to -683) through bioinformatics analysis (Fig. 3A).

To further identify the transcriptional regulation of ZNF667 on these three genes, a ChIP assay was performed. A higher amount of chromatin-containing VASH1 promoter region (-226 to -220) was immunoprecipitated by anti-GFP antibody compared with control IgG in HUVECs transfected with pcDNA3.1-ZNF667 plasmid (Fig. 3B). In ZNF667-overexpressed HUVECs, the mRNA expression of VASH1 decreased by 75%, while no obvious change was observed in the mRNA expression of VEGFA and PFKFB3. Band shift was abolished by specific competitor (Fig. 3D, lane 3), while no obvious change was observed by the addition of mutant VASH1 competitor (Fig. 3D, lane 4). Super shift was observed following incubation with ZNF667 antibody (Fig. 3D, lanes 5 and 6), indicating the specificity of the bound complex. These data strongly suggested that ZNF667 could directly bind to the promoter of VASH1. Next, the regulation was identified through detecting the effect of ZNF667 on VASH1 expression. As shown in Fig. 3C, E and F, overexpression of ZNF667 predominantly decreased the mRNA and protein levels of VASH1. This suggested that ZNF667-regulated angiogenesis might be related to the inhibition of VASH1 transcription.

The expression of VASH1 is downregulated in the ECs of ischemic myocardium following AMI. Although VASH1 is commonly regarded as an angiogenesis inhibitor, its role and correlation with ZNF667 in myocardial ischemia remain to be elucidated. Hence, the expression of VASH1 was detected in the ischemic myocardium and it was found that the expression of VASH1 significantly increased on day 1 and 3 after LAD ligation when compared with sham controls. However, VASH1 expression decreased with the extension of ischemic duration and was negatively associated with the expression of ZNF667 (Fig. 4A and B). VASH1, a protein preferentially expressed in ECs, was also found to be expressed in different types of cells, such as fibroblasts and smooth muscle cells. Consequently, the expressions of CD31 and VASH1 were detected by IHC using serial sections. The results showed that the expression of VASH1 in CD31-positive ECs of ischemic myocardium distinctly decreased (Fig. 4C and D). Taken together, these results suggested that downregulation of VASH1 might be involved in neovascularization following AMI.

Hypoxia-induced downregulation of VASH1 facilitates the invasion and tube formation of HUVECs in vitro. To further explore the role of VASH1 during myocardial ischemia, the expression of VASH1 in HUVECs exposed to hypoxic conditions was detected. It was shown that hypoxic exposure decreased the mRNA and protein expressions of VASH1 in a time-dependent manner (Fig. 5A-C). In addition, downregulation of VASH1 expression by siRNA promoted the invasion and tube formation of HUVECs exposed to normoxic conditions (Fig. 5D, F, G, J and K), whereas overexpression of VASH1 in hypoxic conditions abrogated the hypoxia-enhanced invasion and tube formation of HUVECs (Fig. 5E, H, I, L and M). These data suggested that VASH1 could inhibit hypoxia-induced angiogenesis.

ZNF667 promotes invasion and tube formation of HUVECs through transcriptional repression of VASH1. Based on the regulation of ZNF667 on VASH1 transcription, the effect of VASH1 on ZNF667-mediated angiogenesis was further explored. HUVECs transfected with pcDNA3.1-ZNF667 and/or pcDNA3.1-VASH1 were exposed to normoxic conditions. It was shown that overexpression of ZNF667 by pcDNA3.1-ZNF667 enhanced invasion and tube formation of HUVECs, whereas upregulation of VASH1 expression by pcDNA3.1-VASH1 abolished ZNF667 overexpression-promoted invasion and tube formation of HUVECs (Fig. 6A-D). These data strongly indicate that ZNF667 promotes the invasion and tube formation of HUVECs through negative transcriptional regulation of VASH1.

Wnt signaling pathway may be the downstream effector of ZNF667-suppressed VASH1 transcription. For an improved

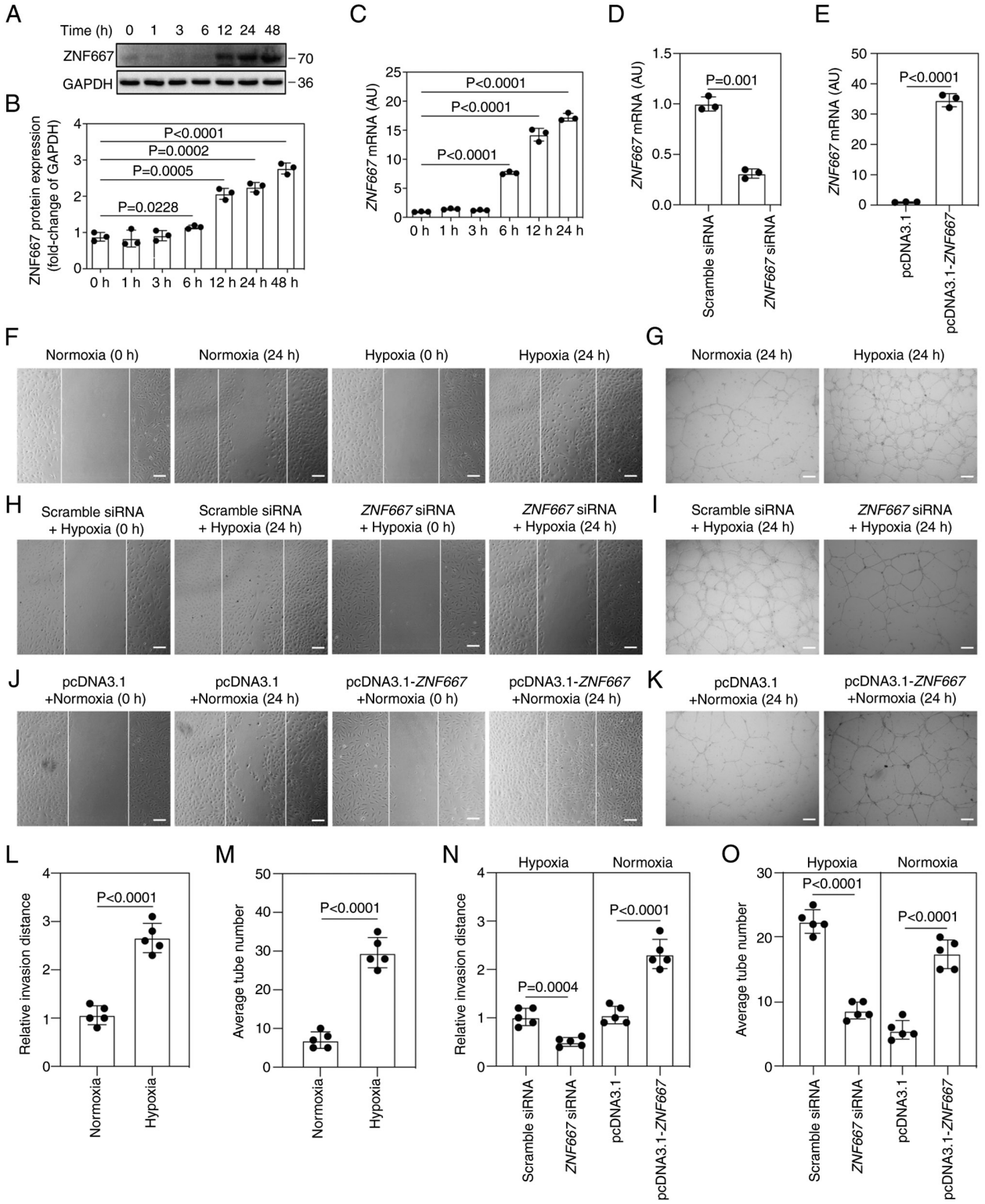

Figure 2. Effect of ZNF667 on the invasion and tube formation of HUVECs exposed to hypoxia. HUVECs cells were cultured *in vitro* and exposed to hypoxic condition for different time. (A) The protein expression of ZNF667 was determined by immunoblotting. (B) Quantification of immunoblot analysis of ZNF667 (n=3 per group). (C) The mRNA expression of ZNF667 in HUVECs was determined by qPCR (n=3 per group). (D) The mRNA expression of ZNF667 in HUVECs transfected with *ZNF667* siRNA or scramble siRNA was determined by qPCR (n=3 per group). (E) The mRNA expression of ZNF667 in HUVECs transfected with pcDNA3.1-*ZNF667* or pcDNA3.1 was determined by qPCR (n=3 per group). (F) Representative micrographs of scratch wound healing assay and (G) *in vitro* Matrigel angiogenesis assay on HUVECs exposed to normoxic or hypoxic conditions; scale bar=100 μm. (H) Representative micrographs of scratch wound healing assay and (I) *in vitro* Matrigel angiogenesis assay on HUVECs transfected with scramble siRNA or ZNF667 siRNA and exposed to hypoxic condition; scale bar=100 μm. (J) Representative micrographs of scratch wound healing assay and (K) *in vitro* Matrigel angiogenesis assay on HUVECs transfected with pcDNA3.1 or pcDN3.1-ZNF667 and exposed to normoxic condition; scale bar=100 μm. (L) Quantitative analysis of scratch wound healing assay and (M) *in vitro* Matrigel angiogenesis assay on HUVECs exposed to normoxic or hypoxic conditions (n=5 per group). Relative invasion distance was analyzed by subtracting the final invasion area for each image (n=5 per group). (N) Quantitative analysis of the scratch wound healing assay and (O) *in vitro* Matrigel angiogenesis assay on HUVECs transfected with scramble siRNA, ZNF667 siRNA, pcDNA3.1, or pcDN3.1-ZNF667 and exposed to hypoxic or normoxic condition (n=5 per group). Data are presented as mean ± standard deviation. ZNF667, zinc finger protein 667; HUVEC, human umbilical vein endothelial cells; siRNA, small interfering RNA.

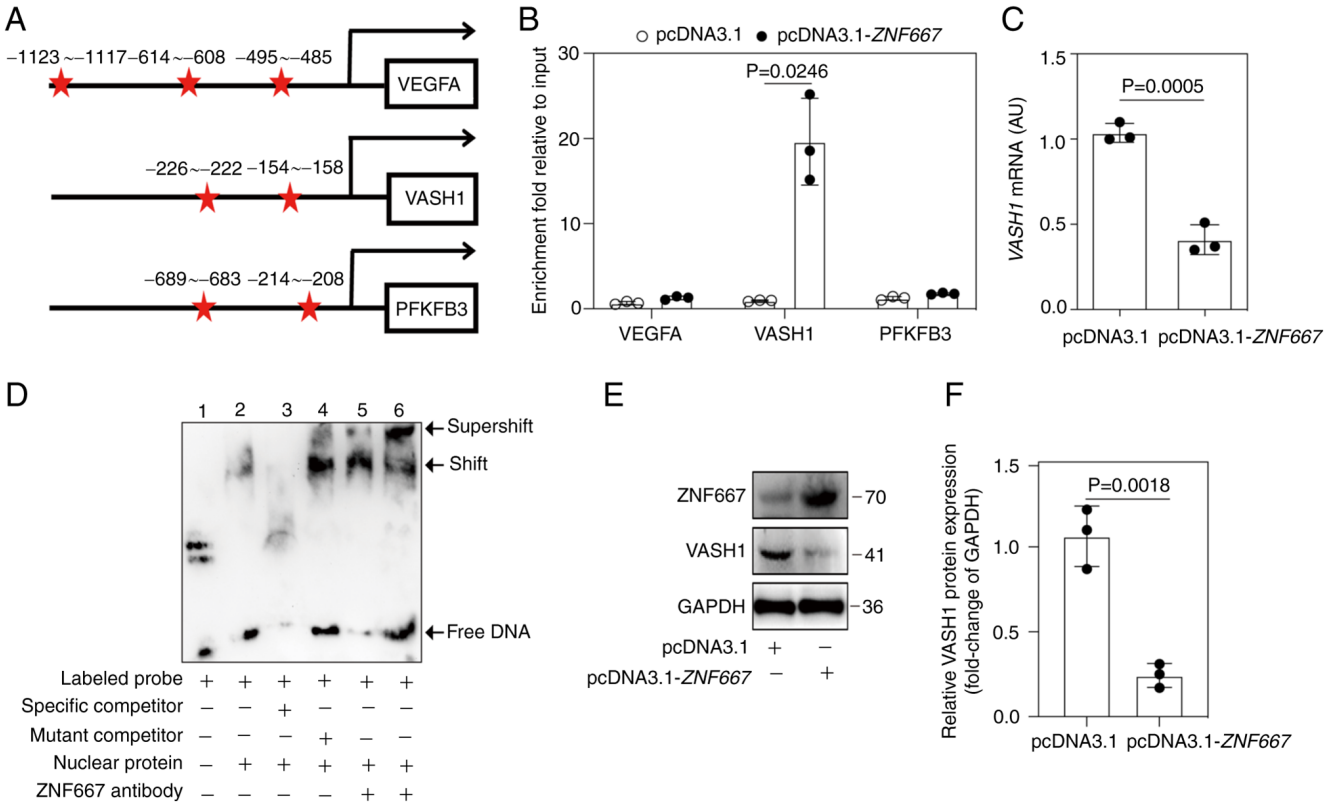

Figure 3. Screening and identification of angiogenesis-related genes regulated by ZNF667. (A) RNA-seq was performed on HUVECs transfected with pcDNA3.1 and pcDNA3.1-ZNF667. Candidate angiogenesis-related genes regulated by ZNF667 were then screened out. Schematic representation of consensus ZNF667 core sequence of the specific DNA binding sites (CTTA; red stars) in the promoter region of candidate angiogenesis-related genes. Arrowheads indicate the orientation of transcription. (B) ChIP assay was performed with cell lysates from HUVECs transfected with pcDNA3.1 and pcDNA3.1-ZNF667. The chromatin was immunoprecipitated with anti-GFP or normal IgG, which served as a negative control. The fold-change of precipitated genomic fragment containing ZNF667 binding site on the VASH1, VEGFA and PFKFB3 promoter was determined by reverse transcription-quantitative PCR. The net quantities of enriched DNA were corrected with their corresponding input DNA. (C) The mRNA expression of VASH1 in HUVECs transfected with pcDNA3.1 and pcDNA3.1-ZNF667 was detected by reverse transcription-quantitative PCR (n=3 per group). (D) ZNF667 protein created a shift (lane 6, arrowed) *in vitro*. EMSA was then performed with 8 μg protein of cell nuclear extracts from hypoxia (1% O_2, 48 h) stimulated cells. (E) The protein expression of VASH1 and ZNF667 in HUVECs transfected with pcDNA3.1 and pcDNA3.1-ZNF667 was detected by immunoblotting. (F) Quantification of immunoblot analysis of ZNF667 and VASH1 (n=3 per group). Data are presented as mean ± standard deviation. RNA-seq, RNA-sequencing; HUVEC, human umbilical vein endothelial cells; ZNF667, zinc finger protein 667; VASH1, vasohibin 1; EMSA, electrophoretic mobility shift assay.

understanding of the landscape of ZNF667-regulated VASH1, gene expression profiling was conducted on two different datasets. One was the GEO GSE27871 microarray dataset derived from HUVECs transfected with VASH1 siRNA (GSE27871). The other one comprised two RNA-seq datasets: untreated HUVECs and HUVECs with ZNF667 overexpression (GSE208105). DEGs between the two RNA-seq datasets were screened out by VennDiagram package. Pair-wise analyses identified 308 co-upregulated DEGs and 95 co-downregulated DEGs from the two datasets (Fig. 7A). To identify the cellular processes commonly affected by ZNF667 upregulation and VASH1 downregulation, biological function distribution analysis of the 403 DEGs was performed using the GO database. Gene set enrichment analysis demonstrated that multiple angiogenic processes were involved, such as extracellular structure organization, cell invasion and blood vessel development (Fig. 7B). Pathway analysis provided a summary view of the potential ZNF667, and VASH1-associated networks and the present study eventually focused on the Wnt signaling pathway, which is often regarded as a proliferative and self-renewal signaling pathway and is also implicated in the processes mentioned above.

In the KEGG pathway analysis, genes such as disheveled-associated activator of morphogenesis 1 (*DAAM1*), lymphoid enhancer-binding factor-1 (*LEF1*), Rac family small GTPase 2 (RAC2), frequently rearranged in advanced T-cell lymphomas-1 (*FRAT1*), phospholipase C beta 2 (*PLCB2*), axin 2 (*AXIN2*), nuclear factor of activated T-cells 2 (NFATc2), CXXC finger protein 4 (CXXC4) and Wnt family member 5A (*WNT5A*) were enriched in the Wnt signaling pathway (P<0.05), indicating that they might be involved in ZNF667-VASH1-reglulated angiogenesis (Fig. 7C). Therefore, the present study further examined the expression of these genes using RT-qPCR. It was found that the mRNA expression of *RAC2*, *LEF1*, *DAAM1*, *NFATc2* and *Wnt5A* was significantly increased in the HUVECs with ZNF667 overexpression. By contrast, the expression of *FRAT1* decreased. *CXXC4*, *AXIN2* and *PLCB2* were ultimately excluded because of their low expression in HUVECs. Notably, HUVECs with VASH1 downregulation exhibited similar effect on the aforementioned genes (Fig. 7D). Taken together, Wnt signaling pathway might be the downstream effector of ZNF667-suppressed VASH1 transcription and further regulate angiogenesis.

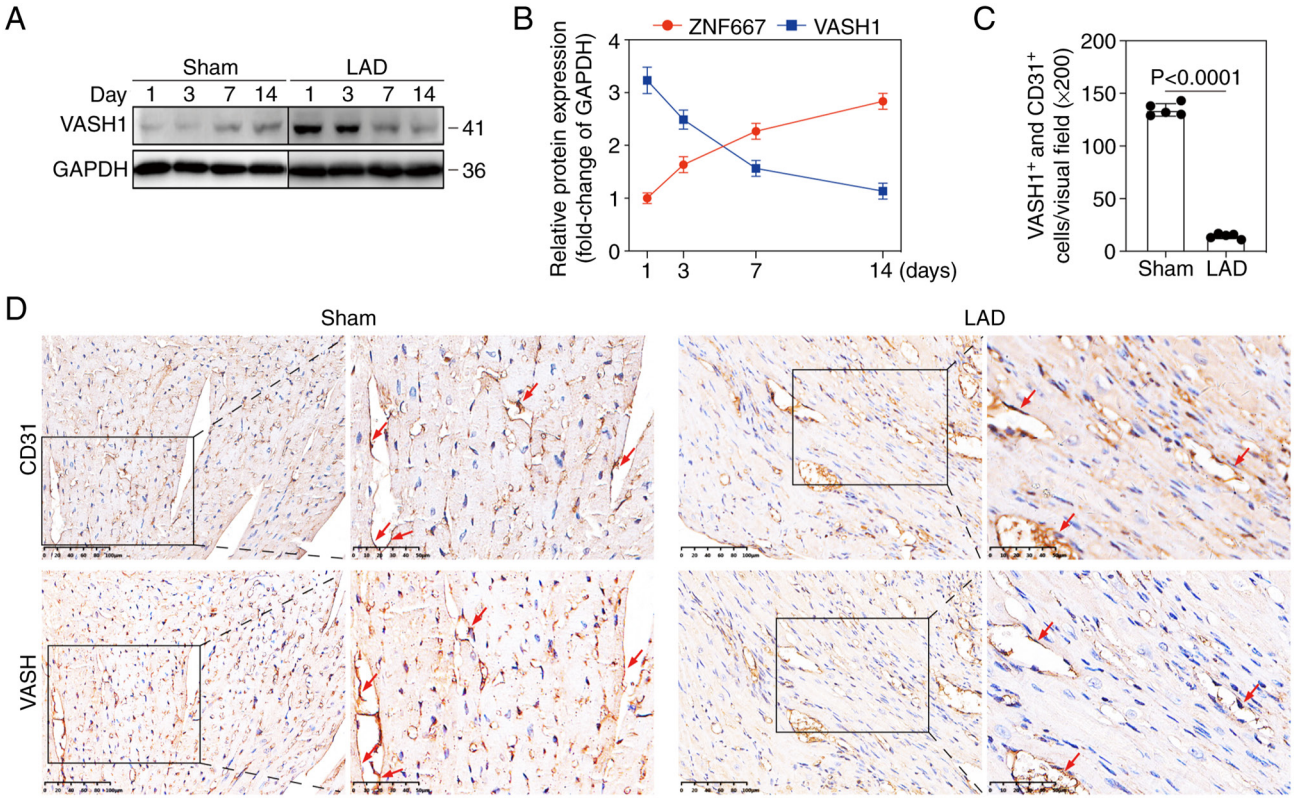

Figure 4. The expression of VASH1 was downregulated in the ECs of ischemic myocardium following AMI. (A) Expression of VASH1 in the left ventricle of mice was detected by immunoblotting on day 1, 3, 7 and 14 following surgery. (B) Correlation of the expression of VASH1 with ZNF667 in the left ventricle of mice on day 1, 3, 7 and 14 day following surgery (n=3 per group). (C) Quantification of positive expression rate of ZNF667 in CD31-positive cells in the left ventricle of AMI mice (n=5 per group). (D) The expression of CD31 and VASH1 were detected by immunohistochemistry in the serial left ventricle sections of AMI mice on day 14 day following surgery. Scale bar (left)=200 μm, (right)=50 μm. The arrows indicate the co-localization of positive expression of CD31 and VASH1. Data are presented as mean ± standard deviation. VASH1, vasohibin 1; EC, endothelial cell; AMI, acute myocardial infarction; ZNF667, zinc finger protein 667.

Discussion

Zinc-finger proteins (ZFPs) are mainly involved in transcriptional regulation, ubiquitin-mediated protein degradation, cell invasion and numerous other processes (32,33). Growing evidence indicates that ZFPs have various cardioprotective effects. For instance, overexpression of zinc-finger protein 418 (ZNF418) protects against cardiac hypertrophy and fibrosis (34). JAZF1, also called zinc finger protein 802 (ZNF802), enhances the proliferation and angiogenesis of cardiac microvascular endothelial cell through the activation of Akt signaling pathway in myocardial ischemia-reperfusion (35). ZNF667, an N-terminal KRAB/C_2H_2 zinc-finger superfamily protein, was identified in our laboratory because of its upregulation during the myocardial ischemic preconditioning process (21). In our previous studies, ZNF667 has been shown to serve an essential role in protecting cardiomyocytes against ischemia-reperfusion or oxidation stress-induced injury (23,25,36,37). In the present study, to investigate the effects of ZNF667 on angiogenesis following AMI and its therapeutic potential, a mouse model of AMI was established through LAD ligation as an ischemia-reperfusion model of mouse heart is unsuitable for the investigation of angiogenesis. For the first time, to the best of the authors' knowledge, ZNF667 was found to be highly expressed in the ECs of ischemic myocardium following AMI. Moreover, hypoxia-induced upregulation of ZNF667 could promote the invasion of tube formation of ECs. These data disclosed a novel role of ZNF667 in AMI.

As a transcription factor, ZNF667 displays a marked anti-apoptotic and cytoprotective effects on cardiomyocytes through transcriptional repression of a series of pro-apoptotic genes, including Fas and Bax (22,23). ZNF667 is upregulated by cerebral ischemic preconditioning and protects astrocytoma cells from oxidative stress (37). ZNF667 also mediates cytoprotection of HIF1 against hydrogen peroxide-mediated injury in H9c2 cells through transcriptional repression of BAX (25). In addition, ZNF667 can inhibit oxLDL-induced foam cell formation, cell apoptosis and lipid accumulation in macrophages by directly inhibiting the transcription of CD36 (38,39). Nonetheless, to date, no angiogenesis-related gene has been identified as the direct target gene of ZNF667. The present study screened out three angiogenesis-related genes as candidate target genes of ZNF667. However, further ChIP assay and EMSA identified VASH1 as the only direct target gene that is involved in the pro-angiogenic effect of ZNF667. ZNF667 can suppress the transcription of VASH1 through directly binding to the specific DNA sequence in its promoter. So far, no direct evidence indicates the role of VASH1 in AMI.

VASH1 was first reported in 2004 by Watanabe *et al* (40), who found that the representative pro-angiogenic growth factors, such as VEGF and fibroblast growth factor 2, can

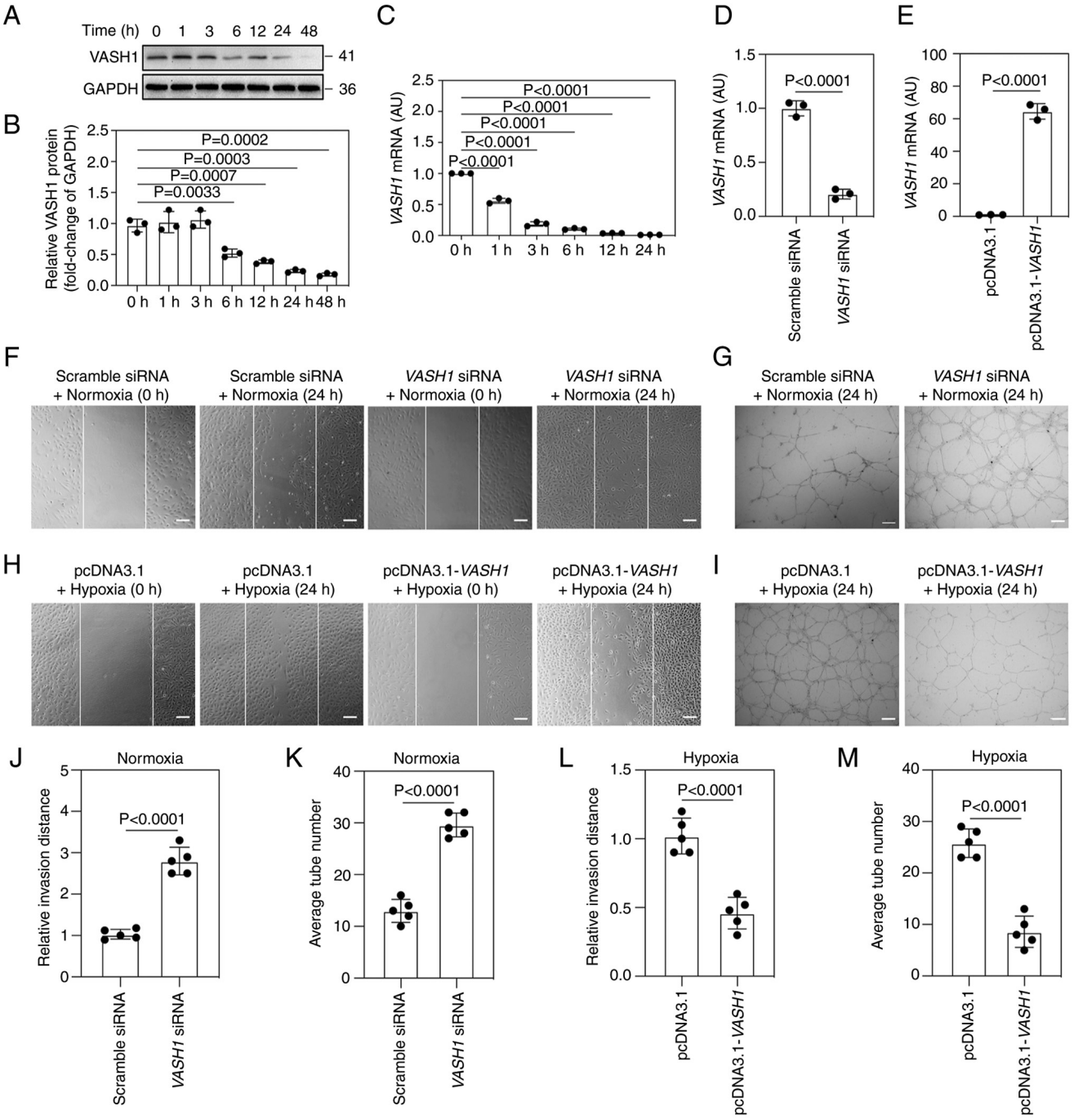

Figure 5. Effect of VASH1 on the invasion and tube formation of HUVECs exposed to hypoxia. HUVECs cells were cultured *in vitro* and exposed to hypoxic condition for different time. (A) The protein expression of VASH1 was determined by immunoblotting. (n=3 per group). (B) Quantification of immunoblot analysis of VASH1 (n=3 per group). (C) The mRNA expression of VASH1 was determined by qPCR. (D) The mRNA expression of *VASH1* in HUVECs transfected with *VASH1* siRNA or scramble siRNA was determined by qPCR (n=3 per group). (E) The mRNA expression of *VASH1* in HUVECs transfected with pcDNA3.1-*VASH1* or pcDNA3.1 was determined by qPCR (n=3 per group). (F) Representative micrographs of scratch wound healing assay and (G) *in vitro* Matrigel angiogenesis assay on HUVECs transfected with scramble siRNA or VASH1 siRNA and exposed to normoxic condition, scale bar=100 μm. (H) Representative micrographs of scratch wound healing assay and (I) *in vitro* Matrigel angiogenesis assay on HUVECs transfected with pcDNA3.1 or pcDNA3.1-*VASH1* and exposed to hypoxic condition, scale bar=100 μm. (J and L) Relative invasion distance was analyzed by subtracting the final invasion area for each image (n=5 per group). (K and M) Quantitative analysis of the tube formation of HUVECs (n=5 per group). Data are presented as mean ± standard deviation. VASH1, vasohibin 1; HUVEC, human umbilical vein endothelial cells; siRNA, small interfering RNA.

induce the expression of VASH1, but VASH1 inhibited angiogenesis. Hence, it is regarded as an endothelium-derived negative feedback regulator of angiogenesis. Subsequent studies demonstrated that VASH1 is implicated in tumorigenesis, atherosclerosis, age-dependent macular degeneration and diabetic retinopathy (40-42). The present study identified that the expression of VASH1 increased rapidly in ischemic myocardium following AMI and it reached a peak on day 1 after LAD ligation but gradually decreased with the extension of ischemic time. This is contrary to ZNF667 and the expression of VASH1 in ischemic myocardium following AMI is negatively associated with ZNF667. It was hypothesized

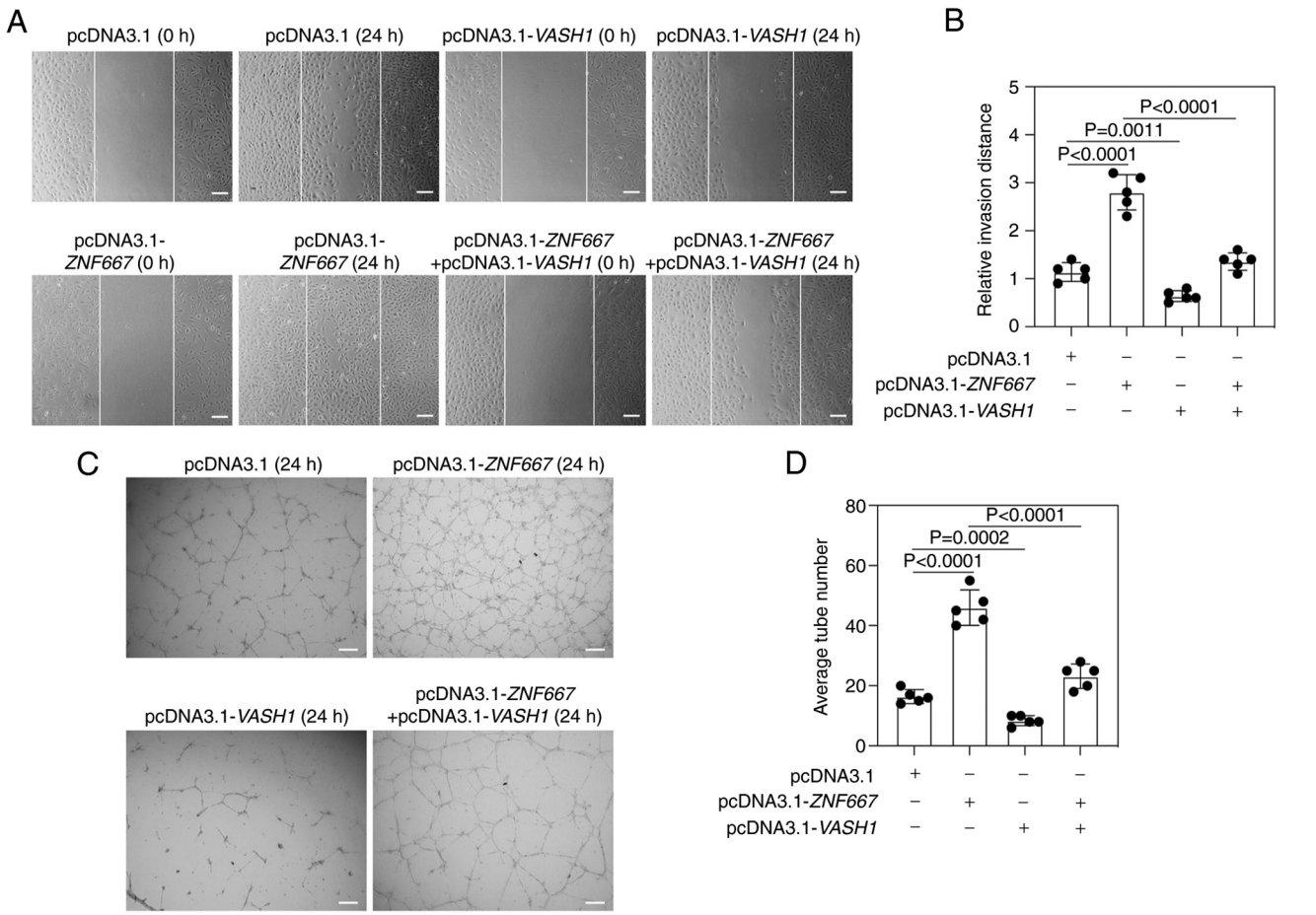

Figure 6. Effect of VASH1 on the invasion and tube formation of HUVECs with ZNF667 overexpression. HUVECs were transfected with scramble pcDNA3.1, pcDNA3.1-VASH1 and/or pcDNA3.1-ZNF667. (A) Representative micrographs of scratch wound healing assay, scale bar=100 μm. (B) Relative invasion distance was analyzed by subtracting the final invasion area for each image (n=5 per group). (C) Representative micrographs of *in vitro* Matrigel angiogenesis assay, scale bar=100 μm. (D) Quantitative analysis of the tube formation of HUVECs (n=5 per group). Data are presented as mean ± standard deviation. VASH1, vasohibin 1; HUVEC, human umbilical vein endothelial cells; ZNF667, zinc finger protein 667.

that the rapid increase in VASH1 may be stimulated by the pro-angiogenic factors aforementioned, while the decrease in VASH1 may be mediated by the increase in ZNF667. Furthermore, hypoxia and ZNF667 overexpression-induced invasion and tube formation of HUVECs, were abolished by VASH1 overexpression. These data indicated that ZNF667 facilitated ischemia/hypoxia-induced angiogenesis through repressing the transcription of VASH1.

To provide insights into the underlying mechanisms of ZNF667-VASH1-regulated angiogenesis, GSE27871 microarray dataset derived from VASH1 siRNA-treated HUVECs and RNA-seq dataset from HUVECs with ZNF667 overexpression were merged. A total of 403 common DEGs in the two datasets were screened out by the VennDiagram package. Subsequent gene set enrichment and pathway analyses indicated that Wnt signaling pathway may mediate the ZNF667-VASH1-regulated angiogenesis. KEGG pathway analysis demonstrated that nine genes were enriched in the Wnt signaling pathway. However, only six genes, including *RAC2*, *LEF1*, *DAAM1*, *NFATc2*, *WNT5A* and *FRAT1* were identified by qPCR. It is known that there are at least three Wnt signaling pathways: The canonical Wnt/β-catenin pathway and two non-canonical pathways, namely Wnt/calcium (Wnt/Ca^{2+}) pathway and Wnt/planar cell polarity pathway (Wnt/PCP) (43). The canonical Wnt/β-catenin pathway facilitates the transcription of a number of Wnt target genes that are involved in cell proliferation and vascular growth (44,45). While activation of non-canonical Wnt/Ca^{2+} pathway has been shown to antagonize Wnt/CTNNB1 signaling transduction through WNT5A-induced activation of the mitogen-activated protein kinase kinase kinase 7 (MAP3K7)-nemo like kinase (NLK) pathway (46). As such, WNT5A is an activator of the non-canonical Wnt pathway and an inhibitor of the canonical Wnt pathway. WNT5A-mediates non-canonical Wnt signaling and can also promote human endothelial cell proliferation and invasion (47). Accumulating evidence indicates that WNT5A exhibits dual effects on angiogenesis, which depends on cell types, receptors, downstream effectors and microenvironment (48). In addition to WNT5A, RAC2, DAAM1 and NFATc2 are the effectors of non-canonical Wnt pathway, while FRAT1 and LEF1 are the effectors of canonical WNT pathway. Expression of RAC2 in ECs is required for the postnatal neovascular response (49). DAAM1 regulates endothelial cell growth, invasion and angiogenesis through microtubule stabilization in a cell type-selective manner (50). NFATc2 acts as a convergence point between stimulatory and inhibitory signals in the regulation of angiogenesis (51,52). LEF1 regulates endothelial cell invasion and thereby the initial steps

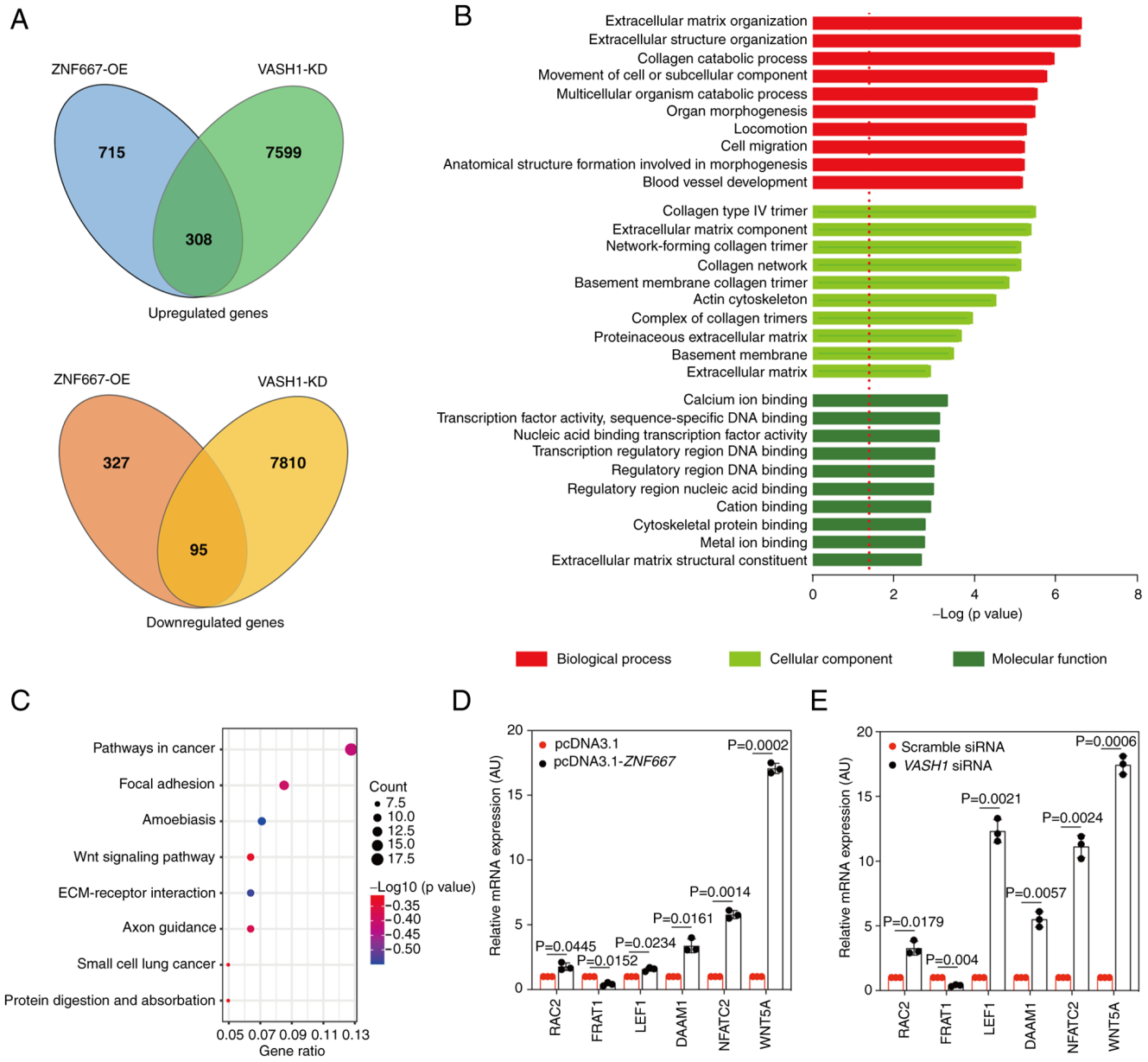

Figure 7. Screening and identification of the gene sets and networks associated with ZNF667-VASH1-regulated angiogenesis. (A) Venn Diagram of VASH1 and ZNF667-associated differentially expressed genes. Top: upregulated genes, bottom: downregulated genes in two gene arrays and RNA sequencing. (B) GO analysis of differentially expressed proteins among different biological processes. The GO terms associated with biological process, molecular function and cellular component of DEGs. (C) KEGG pathway analysis of the top seven networks derived from 403 DEGs in Fig. 7A. (D) The mRNA expression of six candidate genes in HUVECs transfected with pcDNA3.1 or pcDNA3.1-ZNF667 was identified by reverse transcription-quantitative PCR (n=3 per group). (E) The mRNA expression of six candidate genes in HUVECs transfected with pcDNA3.1 or pcDNA3.1-VASH1 was identified by qPCR (n=3 per group). Data are presented as mean ± standard deviation. ZNF667, zinc finger protein 667; VASH1, vasohibin 1; GO, Gene Ontology; KEGG, Kyoto Encyclopedia of Genes and Genomes; DEGs, differentially expressed genes.

of angiogenesis by modulating metalloproteinase-2 expression when targeted by active β-catenin (53). Although the role of FRAT1 in angiogenesis is unclear, it has been proven to be a positive regulator of the Wnt/CTNNB1 signaling pathway in many tumor cells (54). ZNF667 overexpression not only shows positive effects on the transcription of non-canonical Wnt pathway-related genes (*RAC2*, *DAAM1*, *NFAT2* and *WNT5A*), but also shows inhibitory effects on canonical Wnt pathway-related genes (*FRAT1*). Since WNT5A plays an important role in the complex cross-talk between the canonical and non-canonical Wnt signaling pathways, it was hypothesized that WNT5A-mediated signaling pathway may be the downstream effector of ZNF667-suppressed VASH1 transcription and further regulates angiogenesis. However, further studies are required to verify the actual role of these genes in ZNF667-regulated angiogenesis post AMI.

It is noteworthy to mention that inflammatory response serves a critical role in the ventricular remodeling following myocardial infarction. The present study also found that ZNF667 was expressed in the inflammatory cells infiltrated in the myocardium following LAD ligation. Meanwhile, from the RNA-seq data, several inflammation-related genes, such as IL1β, NOD-like receptor protein 3, CD127 and IL18, were found to be upregulated in HUVECs with ZNF667 overexpression.

Our previous study showed that lipopolysaccharide can induce the expression of ZNF667 in different types of tissues, especially in the spleen (55). Therefore, it was hypothesized that ZNF667 may also exert an anti-inflammatory effect during AMI, which can contribute to alleviate ischemic myocardial injury.

In summary, the present study provided conclusive evidence that ZNF667 can facilitate myocardial ischemia-driven angiogenesis through transcriptional regulation of VASH1 and Wnt signaling pathway. ZNF667 serves as a promising molecular target for the treatment of IHD and other angiogenesis-related diseases. However, whether Wnt pathway is indispensable for ZNF667/VASH1 axis-regulated angiogenesis post myocardial ischemia remains to be identified by using Wnt inhibitors (e.g., IWP-2, XAV939) or genetic intervention. Further studies are needed to distinguish the role and potential mechanism of ZNF667 in compensatory or therapeutic angiogenesis and angiogenesis-driven disorders.

Acknowledgements

Not applicable.

Funding

The present study was supported by the grants from National Natural Science Foundation of China (grant nos. 81470408, 81270201 and 81000846), Natural Science Foundation of Hunan Province of China (grant nos. 2020JJ4774 and 2022JJ30786).

Availability of data and materials

The datasets used and/or analyzed during the current study are available from the corresponding author on reasonable request.

Authors' contributions

KW and NW designed the study and confirmed the authenticity of all the raw data. HZ carried out the high-throughput sequencing experiments and provided critical advice during the preparation of the manuscript. Material preparation, data collection and analysis were performed by WW, JZ, KL, ML, XQ and WS. All authors commented on previous versions of the manuscript and read and approved the final manuscript.

Ethics approval and consent to participate

Animal use procedures were approved by the animal welfare ethics committee of Central South University (approval no. 20131502). In addition, all animal protocols conform to the Guide for the Care and Use of Laboratory Animals (8th edition) published by the US National Institute of Health (27).

Patient consent for publication

Not applicable.

Competing interests

The authors declare that they have no competing interests.

References

1. Benjamin EJ, Blaha MJ, Chiuve SE, Cushman M, Das SR, Deo R, de Ferranti SD, Floyd J, Fornage M, Gillespie C, *et al*: Heart disease and stroke statistics-2017 update: A report from the american heart association. Circulation 135: e146-e603, 2017.
2. Lozano R, Naghavi M, Foreman K, Lim S, Shibuya K, Aboyans V, Abraham J, Adair T, Aggarwal R, Ahn SY, *et al*: Global and regional mortality from 235 causes of death for 20 age groups in 1990 and 2010: A systematic analysis for the global burden of disease study 2010. Lancet 380: 2095-2128, 2012.
3. Olivetti G, Capasso JM, Meggs LG, Sonnenblick EH and Anversa P: Cellular basis of chronic ventricular remodeling after myocardial infarction in rats. Circ Res 68: 856-869, 1991.
4. Hori M and Nishida K: Oxidative stress and left ventricular remodelling after myocardial infarction. Cardiovasc Res 81: 457-464, 2009.
5. Ware JA and Simons M: Angiogenesis in ischemic heart disease. Nat Med 3: 158-164, 1997.
6. Cho HM, Kim PH, Chang HK, Shen YM, Bonsra K, Kang BJ, Yum SY, Kim JH, Lee SY, Choi MC, *et al*: Targeted genome engineering to control VEGF expression in human umbilical cord blood-derived mesenchymal stem cells: Potential implications for the treatment of myocardial infarction. Stem Cells Transl Med 6: 1040-1051, 2017.
7. Tykhomyrov AA, Nedzvetsky VS, Bardachenko NI, Grinenko TV and Kuryata OV: Statin treatment decreases serum angiostatin levels in patients with ischemic heart disease. Life Sci 134: 22-29, 2015.
8. Chu H and Wang Y: Therapeutic angiogenesis: Controlled delivery of angiogenic factors. Ther Deliv 3: 693-714, 2012.
9. Ouma GO, Jonas RA, Usman MH and Mohler ER III: Targets and delivery methods for therapeutic angiogenesis in peripheral artery disease. Vasc Med 17: 174-192, 2012.
10. Lavu M, Gundewar S and Lefer DJ: Gene therapy for ischemic heart disease. J Mol Cell Cardiol 50: 742-750, 2011.
11. Yamamoto N, Oyaizu T, Enomoto M, Horie M, Yuasa M, Okawa A and Yagishita K: VEGF and bFGF induction by nitric oxide is associated with hyperbaric oxygen-induced angiogenesis and muscle regeneration. Sci Rep 10: 2744, 2020.
12. Zaslavsky A, Baek KH, Lynch RC, Short S, Grillo J, Folkman J, Italiano JE Jr and Ryeom S: Platelet-derived thrombospondin-1 is a critical negative regulator and potential biomarker of angiogenesis. Blood 115: 4605-4613, 2010.
13. Matsunaga T, Weihrauch DW, Moniz MC, Tessmer J, Warltier DC and Chilian WM: Angiostatin inhibits coronary angiogenesis during impaired production of nitric oxide. Circulation 105: 2185-2191, 2002.
14. Idrisova KF, Zeinalova AK, Masgutova GA, Bogov AA, Allegrucci C, Syromiatnikova VY, Salafutdinov II, Garanina EE, Andreeva DI, Kadyrov AA, *et al*: Application of neurotrophic and proangiogenic factors as therapy after peripheral nervous system injury. Neural Regen Res 17: 1240-1247, 2022.
15. Almeida I, Gomes AO, Lima M, Silva I and Vasconcelos C: Different contributions of angiostatin and endostatin in angiogenesis impairment in systemic sclerosis: A cohort study. Clin Exp Rheumatol 100 (Suppl): 37-42, 2016.
16. Zhao G, Na R, Li L, Xiao H, Ding N, Sun Y and Han R: Vasohibin-1 inhibits angiogenesis and suppresses tumor growth in renal cell carcinoma. Oncol Rep 38: 1021-1028, 2017.
17. Tang X, Yang Y, Yuan H, You J, Burkatovskaya M and Amar S: Novel transcriptional regulation of VEGF in inflammatory processes. J Cell Mol Med 17: 386-397, 2013.
18. Matsakas A, Yadav V, Lorca S, Evans RM and Narkar VA: Revascularization of ischemic skeletal muscle by estrogen-related receptor-gamma. Circ Res 110: 1087-1096, 2012.
19. Arany Z, Foo SY, Ma Y, Ruas JL, Bommi-Reddy A, Girnun G, Cooper M, Laznik D, Chinsomboon J, Rangwala SM, *et al*: HIF-independent regulation of VEGF and angiogenesis by the transcriptional coactivator PGC-1alpha. Nature 451: 1008-1012, 2008.
20. Lu C, Han HD, Mangala LS, Ali-Fehmi R, Newton CS, Ozbun L, Armaiz-Pena GN, Hu W, Stone RL, Munkarah A, *et al*: Regulation of tumor angiogenesis by EZH2. Cancer Cell 18: 185-197, 2010.

21. Yuan C, Zhang HL, Liu Y, Wang QP and Xiao XZ: Cloning and characterization of a new gene mip1 up-regulated during myocardial ishemia-reperfusion. Progress in Biochemistry and Biophysics 2004: 231-236, 2014 (In Chinese).
22. Wang G, Jiang L, Song J, Zhou SF, Zhang H, Wang K and Xiao X: Mipu1 protects H9c2 myogenic cells from hydrogen peroxide-induced apoptosis through inhibition of the expression of the death receptor Fas. Int J Mol Sci 15: 18206-18220, 2014.
23. Jiang L, Wang H, Shi C, Liu K, Liu M, Wang N, Wang K, Zhang H, Wang G and Xiao X: ZNF667/Mipu1 is a novel anti-apoptotic factor that directly regulates the expression of the rat Bax gene in H9c2 cells. PLoS One 9: e111653, 2014.
24. Wang G, Zuo X, Yuan C, Zheng Y, Jiang L, Song J, Liu Y, Zhang B and Xiao X: Mipu1, a novel rat zinc-finger protein, inhibits transcriptional activities of AP-1 and SRE in mitogen-activated protein kinase signaling pathway. Mol Cell Biochem 322: 93-102, 2009.
25. Wang K, Lei J, Zou J, Xiao H, Chen A, Liu X, Liu Y, Jiang L, Xiao Z and Xiao X: Mipu1, a novel direct target gene, is involved in hypoxia inducible factor 1-mediated cytoprotection. PLoS One 8: e82827, 2013.
26. Hashimoto T and Shibasaki F: Hypoxia-inducible factor as an angiogenic master switch. Front Pediatr 3: 33, 2015.
27. National Research Council (US) Committee for the Update of the Guide for the Care and Use of Laboratory Animals: Guide for the Care and Use of Laboratory Animals. National Academies Press, Washington, DC, 2011.
28. Zou J, Wang N, Liu M, Bai Y, Wang H, Liu K, Zhang H, Xiao X and Wang K: Nucleolin mediated pro-angiogenic role of Hydroxysafflor Yellow A in ischaemic cardiac dysfunction: Post-transcriptional regulation of VEGF-A and MMP-9. J Cell Mol Med 22: 2692-2705, 2018.
29. Zou J, Fei Q, Xiao H, Wang H, Liu K, Liu M, Zhang H, Xiao X, Wang K and Wang N: VEGF-A promotes angiogenesis after acute myocardial infarction through increasing ROS production and enhancing ER stress-mediated autophagy. J Cell Physiol 234: 17690-17703, 2019.
30. Jiang L, Tang D, Wang K, Zhang H, Yuan C, Duan D and Xiao X: Functional analysis of a novel KRAB/C2H2 zinc finger protein Mipu1. Biochem Biophys Res Commun 356: 829-835, 2007.
31. Livak KJ and Schmittgen TD: Analysis of relative gene expression data using real-time quantitative PCR and the 2(-Delta Delta C(T)) method. Methods 25: 402-408, 2001.
32. Cassandri M, Smirnov A, Novelli F, Pitolli C, Agostini M, Malewicz M, Melino G and Raschellà G: Zinc-finger proteins in health and disease. Cell Death Discov 3: 17071, 2017.
33. Laity JH, Lee BM and Wright PE: Zinc finger proteins: New insights into structural and functional diversity. Curr Opin Struct Biol 11: 39-46, 2001.
34. Pan L, Sheng M, Huang Z, Zhu Z, Xu C, Teng L, He L, Gu C, Yi C and Li J: Zinc-finger protein 418 overexpression protects against cardiac hypertrophy and fibrosis. PLoS One 12: e0186635, 2017.
35. Shang J, Gao ZY, Zhang LY and Wang CY: Over-expression of JAZF1 promotes cardiac microvascular endothelial cell proliferation and angiogenesis via activation of the Akt signaling pathway in rats with myocardial ischemia-reperfusion. Cell Cycle 18: 1619-1634, 2019.
36. Wang G, Zuo X, Liu J, Jiang L, Liu Y, Zheng Y, Zhang B and Xiao X: Expression of Mipu1 in response to myocardial infarction in rats. Int J Mol Sci 10: 492-506, 2009.
37. Yuan D, Huang J, Yuan X, Zhao J and Jiang W: Zinc finger protein 667 expression is upregulated by cerebral ischemic preconditioning and protects cells from oxidative stress. Biomed Rep 1: 534-538, 2013.
38. Qu SL, Fan WJ, Zhang C, Guo F, Pan WJ, Han D, Li W, Zhu YN and Jiang ZS: Mipu1 inhibits lipid accumulation through down-regulation of CD36 in RAW264.7 cells. Cell Physiol Biochem 37: 879-889, 2015.
39. Qu SL, Fan WJ, Zhang C, Guo F, Han D, Pan WJ, Li W, Feng DM and Jiang ZS: Mipu1 overexpression protects macrophages from oxLDL-induced foam cell formation and cell apoptosis. DNA Cell Biol 33: 839-846, 2014.
40. Watanabe K, Hasegawa Y, Yamashita H, Shimizu K, Ding Y, Abe M, Ohta H, Imagawa K, Hojo K, Maki H, *et al*: Vasohibin as an endothelium-derived negative feedback regulator of angiogenesis. J Clin Invest 114: 898-907, 2004.
41. Kimura H, Miyashita H, Suzuki Y, Kobayashi M, Watanabe K, Sonoda H, Ohta H, Fujiwara T, Shimosegawa T and Sato Y: Distinctive localization and opposed roles of vasohibin-1 and vasohibin-2 in the regulation of angiogenesis. Blood 113: 4810-4818, 2009.
42. Takahashi Y, Saga Y, Koyanagi T, Takei Y, Machida S, Taneichi A, Mizukami H, Sato Y, Matsubara S and Fujiwara H: The angiogenesis regulator vasohibin-1 inhibits ovarian cancer growth and peritoneal dissemination and prolongs host survival. Int J Oncol 47: 2057-2063, 2015.
43. Miller JR: The wnts. Genome Biol 3: REVIEWS3001, 2002.
44. Tetsu O and McCormick F: Beta-catenin regulates expression of cyclin D1 in colon carcinoma cells. Nature 398: 422-426, 1999.
45. Zhang X, Gaspard JP and Chung DC: Regulation of vascular endothelial growth factor by the Wnt and K-ras pathways in colonic neoplasia. Cancer Res 61: 6050-6054, 2001.
46. Ishitani T, Kishida S, Hyodo-Miura J, Ueno N, Yasuda J, Waterman M, Shibuya H, Moon RT, Ninomiya-Tsuji J and Matsumoto K: The TAK1-NLK mitogen-activated protein kinase cascade functions in the Wnt-5a/Ca(2+) pathway to antagonize Wnt/beta-catenin signaling. Mol Cell Biol 23: 131-139, 2003.
47. Cheng CW, Yeh JC, Fan TP, Smith SK and Charnock-Jones DS: Wnt5a-mediated non-canonical Wnt signalling regulates human endothelial cell proliferation and migration. Biochem Biophys Res Commun 365: 285-290, 2008.
48. Shi YN, Zhu N, Liu C, Wu HT, Gui Y, Liao DF and Qin L: Wnt5a and its signaling pathway in angiogenesis. Clin Chim Acta 471: 263-269, 2017.
49. De P, Peng Q, Traktuev DO, Li W, Yoder MC, March KL and Durden DL: Expression of RAC2 in endothelial cells is required for the postnatal neovascular response. Exp Cell Res 315: 248-263, 2009.
50. Ju R, Cirone P, Lin S, Griesbach H, Slusarski DC and Crews CM: Activation of the planar cell polarity formin DAAM1 leads to inhibition of endothelial cell proliferation, migration, and angiogenesis. Proc Natl Acad Sci USA 107: 6906-6911, 2010.
51. Cai Y, Yao H, Sun Z, Wang Y, Zhao Y, Wang Z and Li L: Role of NFAT in the progression of diabetic atherosclerosis. Front Cardiovasc Med 8: 635172, 2021.
52. Zaichuk TA, Shroff EH, Emmanuel R, Filleur S, Nelius T and Volpert OV: Nuclear factor of activated T cells balances angiogenesis activation and inhibition. J Exp Med 199: 1513-1522, 2004.
53. Planutiene M, Planutis K and Holcombe RF: Lymphoid enhancer-binding factor 1, a representative of vertebrate-specific Lef1/Tcf1 sub-family, is a Wnt-beta-catenin pathway target gene in human endothelial cells which regulates matrix metalloproteinase-2 expression and promotes endothelial cell invasion. Vasc Cell 3: 28, 2011.
54. Guo G, Liu J, Ren Y, Mao X, Hao Y, Zhong C, Chen X, Wang X, Wu Y, Lian S, *et al*: FRAT1 enhances the proliferation and tumorigenesis of CD133(+)nestin(+) glioma stem cells in vitro and in vivo. J Cancer 11: 2421-2430, 2020.
55. Gao M, Wang H, Liu Y, Tu ZZ, Liu MD, Chen GW and Liu K: Changes of the expression of Mipu1 gene in tissues of mice in endotoxemia. Life Sci Res 14: 331-334, 2010.